



Measurement of acetylene concentration in laminar flat flames by diode laser cavity ring-down spectroscopy

P. Otti¹ · G. S. Humphries^{1,2} · Y. Hu¹ · M. Lengden² · I. S. Burns¹

Received: 30 March 2022 / Accepted: 1 August 2022 / Published online: 12 August 2022
© The Author(s), under exclusive licence to Springer-Verlag GmbH Germany, part of Springer Nature 2022

Abstract

Continuous-wave cavity ring-down spectroscopy (cw-CRDS) has been applied to measure trace gas concentration in situ in flames using a near-infrared diode laser. Acetylene concentration was measured in laminar flat flames of premixed ethylene and air at atmospheric pressure for a range of fuel–air ratios. This was achieved by recording CRDS spectra of the P17e feature of acetylene near 1535 nm. The resulting concentration profiles show higher acetylene concentrations for increasing equivalence ratio. Downstream of the reaction zone, a trend of decreasing acetylene concentration with increasing height above the burner surface was observed in each of the flames studied. This would be consistent with the consumption of acetylene in the formation and growth of polycyclic aromatic hydrocarbons (PAHs) and soot. Extinction data are also reported and reveal significant broadband optical losses in the richer flames, including prior to the onset of soot formation, which may be attributable to near-infrared absorption by aromatic species.

1 Introduction

The emission of soot and aromatic hydrocarbons from transportation and stationary combustion processes is currently under significant world-wide scrutiny, due to the harmful effects on human health [1, 2] and the impact on climate change [3]. This has led to an increased research effort into understanding the formation of these species during the combustion process [4, 5]. Much of this work is directed towards the development of physicochemical mechanisms of soot and polycyclic aromatic hydrocarbon (PAH) formation in flames [6]. A key requirement for the development of such mechanisms is the in situ measurement of soot, PAH and precursor species in combustion geometries which have a simple flow-field with well-defined boundary conditions [7]. Simple lab-scale burners, such as flat flames allow the implementation of sophisticated optical diagnostic techniques with sufficient sensitivity to accurately measure the

concentration profiles of important precursor species in the PAH formation process.

One such soot precursor is acetylene (C_2H_2), which is regarded as having a fundamental role in soot formation for two reasons. First, it is critical to the hydrogen abstraction– C_2H_2 addition (HACA) mechanism [4], by which PAH molecules grow towards larger numbers of aromatic rings. Acetylene is also involved at an earlier stage in the combustion process, leading to the formation of the first aromatic ring. Various chemical pathways are thought to lead to the formation of benzene and propargyl (C_3H_3) is one of the important intermediates [8]. A reaction which contributes significantly to the formation of propargyl is the reaction of acetylene with singlet methylene ($^1CH_2 + C_2H_2 \rightarrow C_3H_3 + H$) [9]. Consequently, the availability of experimental reference data for acetylene concentration in flames is vital for validation of soot formation models.

Several optical measurement techniques have previously been demonstrated to measure acetylene spectra in flames, including direct absorption spectroscopy [10], Raman spectroscopy [11], laser-induced fluorescence (LIF) [12], coherent anti-Stokes Raman Spectroscopy (CARS) [13] and polarisation spectroscopy [14, 15]. There has also been a previous demonstration of cavity ring-down spectroscopy (CRDS) of acetylene using a pulsed optical parametric oscillator (OPO) at 3.1 μm [16].

✉ I. S. Burns
iain.burns@strath.ac.uk

¹ Department of Chemical and Process Engineering,
University of Strathclyde, Montrose Street, Glasgow G1 1XJ,
Scotland, UK

² Department of Electronic and Electrical Engineering,
University of Strathclyde, George Street, Glasgow G1 1XW,
Scotland, UK

The techniques of Raman scattering, LIF, CARS, PS and pulsed CRDS all require high-power, pulsed lasers and often require the use of non-linear frequency conversion to the UV, near-infrared or mid-infrared. This involves large and bulky equipment typically consisting of an Nd:YAG laser together with a tunable dye laser or OPO. Compared to the use of diode lasers, the resulting infrared pulses generally have a much broader linewidth, often as large as a wavenumber, which means that narrow spectral lines may be under-resolved. This poses a particular problem for measurements in complex environments such as flames, where the composition of the combustion environment leads to a high number of interfering absorption features corresponding to a number of different species. As a consequence of these difficulties, there remains no widespread technique used for studies of acetylene in situ in flames.

Many combustion studies [17–20] have instead used extractive sampling techniques for acetylene concentration determination. This approach, however, carries the well-known disadvantages that the presence of a sampling probe will influence the flow-field and temperature profile of the flame [21–23], and thus also perturb the acetylene concentration profile. Continued reactions through the sampling line can also affect measurements, particularly of intermediate species such as acetylene. The spatial resolution of extractive sampling methods is also inferior to what can be achieved with in situ optical diagnostic techniques. Some previous studies [18, 24] have combined the use of extractive sampling with continuous-wave cavity ring-down spectroscopy. In this research, gas was pumped from the flame into a reduced-pressure sample chamber, which formed an optical cavity, allowing the detection of acetylene and other species such as HCN.

An approach that combines the practicality of low-power diode lasers with the benefits of an in situ technique and favourable sensitivity would, therefore, have a useful role in studies of sooting flames. We have previously presented research on the concept of using in situ continuous-wave cavity ring-down to measure acetylene spectra using near-infrared diode lasers [25]. The approach has now been further developed to the point of practical application to measure acetylene concentration profiles in laminar sooting flames. The method presented here excludes the use of a second diode laser and an optical switching system, and thus simplifies the technique. All the data reported in this paper were obtained using this revised approach. We present spectra of acetylene and concentrations derived from these spectra for a range of flame compositions and as a function of height above the burner.

The remainder of this paper is structured as follows. We describe the experimental methodology with the emphasis on a number of refinements to the approach used. This is followed by an explanation of how quantitative concentration

measurements were obtained from the recovered spectra. Experimental results are then presented, including acetylene concentration profiles in rich ethylene-air flames at a range of fuel–air ratios. In addition, we present measurements of broadband extinction for a range of heights above the burner (HAB) in flames ranging from stoichiometric to highly sooting flames.

2 Experimental method

The key components of the modified cw-CRDS setup are shown in Fig. 1. The cw-CRDS methodology employed in this work differs from most other cw-CRDS systems through the use of a semiconductor optical amplifier (SOA, Kameilian, C-Band, maximum power: 20 mW) [26]. This fibre-coupled component serves both as the switching element used to instigate ring-down within the optical cavity, and also amplifies the laser output power. Semiconductor optical amplifiers provide a very high extinction ratio (typically 50 dB) and a fast cut-off time (~ 1 ns), which, therefore, comfortably satisfy the requirements for this application.

The seed source for the SOA is a distributed feedback (DFB) diode laser with a centre wavelength of approximately 1535 nm (maximum output power: 15 mW). The laser is controlled by a laser diode controller (Thorlabs: LDC 210C) and a temperature controller (Thorlabs: TED200C). Using a NI LabView program and a NI DAQ card (National Instruments: PCI 6120), the laser was incrementally current-tuned over a wavelength range of approximately 1535.30–1535.55 nm to interrogate the P17e transition of acetylene. The relative wavelength of the laser over this

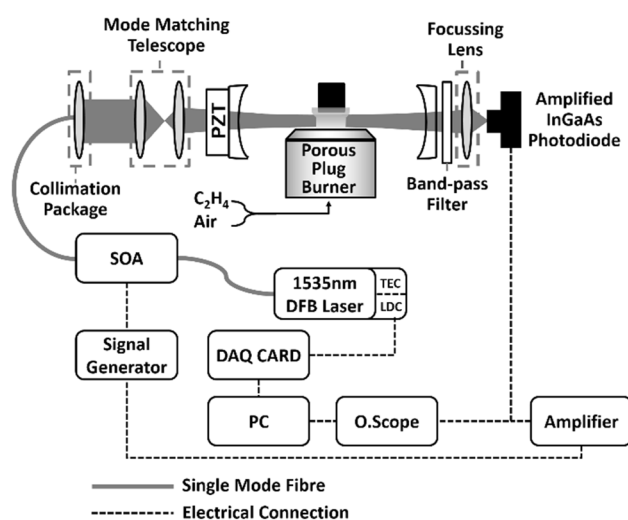


Fig. 1 Experimental setup for cw-CRDS: SOA semiconductor optical amplifier, DAQ Card multifunction data acquisition card, TEC thermoelectric controller, LDC laser diode controller

scanning range was measured using a fibre ring-resonator with a free-spectral range of 0.428 GHz [27]. At each wavelength increment, ring-down traces were recorded and averaged. Between each current increment, the laser wavelength was tuned to an off-resonance reference wavelength of 1535.34 nm (corresponding to a drive current of 115 mA), at which negligible narrow-band absorption is observed, and a similar averaged ring-down trace was recorded. This allowed any long-term drift in the cavity finesse or change in the broadband absorption to be monitored and compensated for when calculating the absorption coefficient. Figure 2 shows the ring-down time spectrum obtained during a laser current scan, together with the corresponding off-resonance ring-down times recorded at the reference wavelength. This methodology is a simplification to our original design, in which a second DFB laser and an optical switching system were used for the same purpose [25]. The off-resonance ring-down time trace shown in Fig. 2 is rather flat, providing useful confirmation that any effects of drift in the cavity alignment or deposition on the mirrors were minor during the timescale of the wavelength scan.

The output beam from the SOA is collimated and coupled into the cavity, via the input mirror, in the fundamental transverse mode (TEM_{00}). This is achieved using a two-lens, Keplerian mode-matching telescope arrangement (focal lengths 60 mm and 30 mm, respectively). The cavity is formed of two high-reflectivity mirrors (CRD Optics; $R = 99.995\%$ at 1550 nm; radius of curvature = 1 m; cavity length: 500 mm). This resulted in a calculated beam waist ($1/e^2$ radius) of 465 μm at the centre of the cavity. The light exiting the cavity through the output mirror passes through a band-pass filter (Thorlabs, 1550 nm, FWHM: 40 nm), which

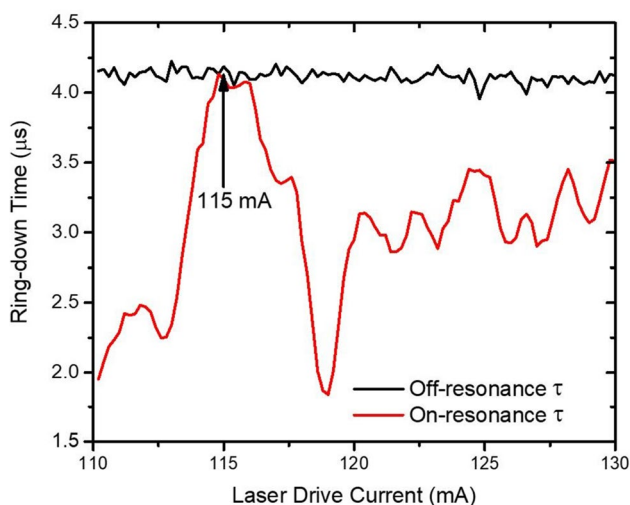


Fig. 2 A ring-down time spectrum recorded during a laser current scan and corresponding off-resonance ring-down times at the reference wavelength (corresponding to an injection current of 115 mA), in a $\phi = 2.07$ flame at 2 mm height above the burner surface

serves to attenuate any emission from the flame which is transmitted through the output cavity mirror. The output light is detected using an amplified InGaAs photodiode (Thorlabs, PDA10CS).

The input mirror is held within a mount that can be piezoelectrically translated through a distance corresponding to roughly half of the laser wavelength. Sinusoidal modulation of the cavity length at a frequency of 50 Hz results in the excitation of a longitudinal resonance twice per modulation cycle. The output from the InGaAs detector is connected to a variable gain high-speed amplifier (Femto: DHCPA-100). A ring-down event is triggered when the optical power circulating within the cavity has reached a pre-set level. Once this threshold is reached, the output from the signal generator driving the SOA is reduced to 0 V, switching off the SOA and allowing the light which has built up inside the cavity to ring-down. The bandwidth of all the sub-systems (detector, amplifier, signal generator, SOA) is high enough to extinguish the incident beam on the timescale required. The ring-down event is monitored with the same InGaAs detector and amplifier, and 32 ring-down traces were averaged for each wavelength increment using an oscilloscope (Tektronix: TDS3014B). The amplification afforded by the SOA in this process increases the optical power circulating when the cavity is resonant, thus improving the signal-to-noise ratio (SNR) of the measured ring-down signal, especially at the low end of the laser current scan. This may be seen as a significant advantage for flame measurements compared to an acousto-optic modulator (AOM), which is more commonly used as an optical switch for cw-CRDS.

Measurements were made in atmospheric pressure flat flames of premixed ethylene and air stabilised on a water-cooled, 33-mm porous-plug of sintered stainless steel. A flat-flame burner was chosen as it is particularly suited for path-integrated optical measurement techniques, such as cw-CRDS as the flame is deemed to be one dimensional, and therefore, there is assumed to be minimal change in the local flame conditions along the beam-path. The ethylene and air flowrates through the burner were controlled using mass-flow controllers (Cole-Palmer) and a total flow rate of 3.10 slpm (i.e. litres per minute at 293 K and 1.01 Pa) was used for the range of flame conditions studied. A stabilisation plate, consisting of a 38 mm diameter stainless-steel cylinder, was fixed 21 mm above the burner [28, 29]. The burner was mounted on an adjustable stage, allowing vertical translation.

3 Determination of acetylene concentration

The cavity ring-down time, $\tau(\nu)$, was obtained at each wavelength increment from each averaged intensity decay trace by fitting an exponential decay function to

the recorded data. The single-pass absorption coefficient, α , was evaluated for each wavelength using the following equation [30]:

$$\alpha(\nu) = \frac{L_c}{cd} \left(\frac{1}{\tau(\nu)} - \frac{1}{\tau_0} \right) \quad (1)$$

where L_c is the cavity length, τ_0 is the ring-down time of the cavity with no absorbing species present (in this case at the reference wavelength), c is the speed of light and d is the absorption path-length, taken as the burner diameter of 33 mm. The absolute wavelength scale was obtained using the centre wavelength of the P17e feature of acetylene from HITRAN. This was assigned to the peak of the experimental P17e feature of the spectrum recorded at $\phi = 2.37$, and HAB of 2 mm, as an initial part of the spectral fitting process (see below). For all the other spectra, slight shifts in the wavelength scale were compensated by exploiting the overlap in the strong flank seen at the right of Fig. 3a, which we assign to water vapour and is present in all recorded spectra.

Spectra recorded for rich flames with a range of equivalence ratios (ϕ) at a height above burner of 2 mm are shown in Fig. 3, together with a spectrum recorded in a stoichiometric flame. Note that the equivalence ratio is defined as the fuel–air ratio divided by the stoichiometric fuel–air ratio. For the rich flames, the measured spectra show similar features to the model spectrum of acetylene (shown in lower plot of Fig. 3), especially for the region near to the strong P17e acetylene feature (at 1535.39 nm). Notably, the experimental spectra also show a high degree of overlap at wavelengths where, according to the model spectrum, there is no contribution from acetylene. This strong agreement is observed for spectra recorded across the range of measurement positions in the flame. This appears to indicate that the spectra, although recorded at different equivalence ratios, share several common absorption features. These non-acetylene absorption features, therefore, seem to be for one or more species whose concentrations do not change substantially for the different equivalence ratios investigated. It is known that water vapour possesses many high-temperature absorption lines in this wavelength range [31] (while the HITRAN database shows no absorption lines for other flame species in this wavelength range) and we, therefore, attribute these features to water vapour. Accordingly, the spectra recorded over a range of flame equivalence ratios appear to differ only due to the contribution of acetylene. Based on this interpretation, a spectrum recorded in the stoichiometric flame, which should contain a negligible concentration of acetylene, is subtracted from each of the spectra recorded in richer flames, yielding a spectrum which is assumed to be attributed to acetylene alone and shown in Fig. 3 (lower plot).

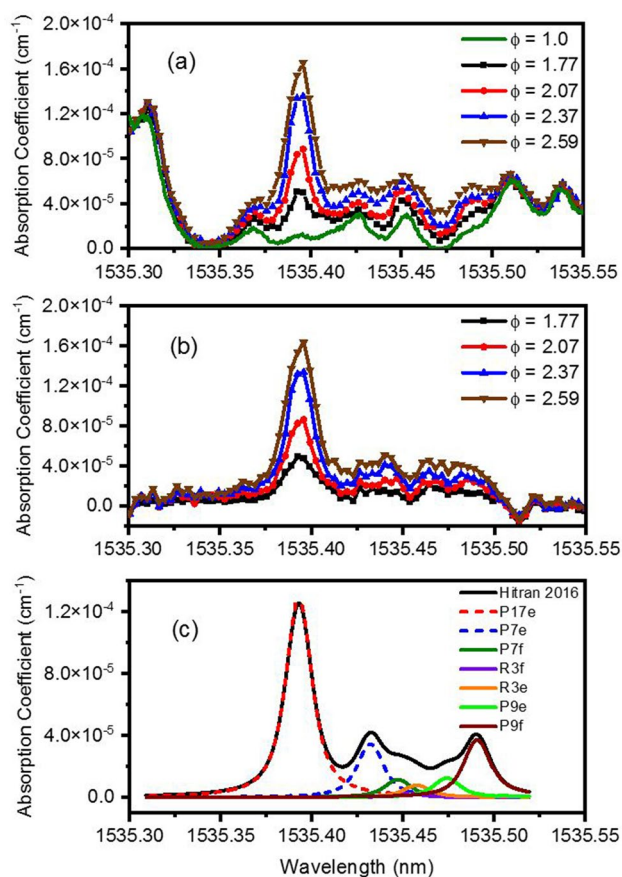


Fig. 3 **a** Spectra of P17e line of acetylene for a range of different equivalence ratio flames recorded 2 mm above the burner surface. **b** Subtracted spectra for a range of different equivalence ratio flames recorded 2 mm above the burner surface. **c** Simulated spectrum of C₂H₂ for a concentration of 1.22%, at 1600 K and atmospheric pressure, with separate Voigt profiles representing seven individual acetylene lines also shown

A spectral model was developed to determine acetylene concentration from the resulting spectra using a least-squares fitting routine. In this model, a theoretical acetylene spectrum is generated using data from the HITRAN2016 database (as shown in Fig. 3) [32]. The least-squares fitting process only considers experimental data in the region of the P17e acetylene feature, between 1535.37 and 1535.42 nm, since this is where the acetylene absorption is strongest. Whilst spectra like those shown in Fig. 3 have been recorded for each flame location, this analysis shows that narrower spectra covering only 1535.37–1535.42 nm are sufficient for concentration evaluation, thus allowing a reduction in the time for data acquisition. The spectral model consists of a sum of two Voigt profiles representing the P17e and P7e acetylene lines, since these are the only ones that show non-negligible absorption within the fitted spectral region (as seen in Fig. 2).

The measured absorption coefficient, $\alpha(\nu)$, may be expressed as a summation of contributions from each of the spectral lines:

$$\alpha(\nu) = \sum_{i=1,2} \sigma_i(\nu)N_i \tag{2}$$

where $\sigma_i(\nu)$ is the absorption cross-section of spectral line i and N_i is the number density in the ground state of the relevant transition. The absorption cross-section can be expressed as

$$\sigma_i(\nu) = \phi(\nu - \nu_i) \int_0^\infty \sigma_i(\nu) d\nu \tag{3}$$

where ν_i is the transition line-centre and $\phi(\nu)$ is a line shape function, whose integral is unity. The Voigt line shape is the convolution of Gaussian and Lorentzian line shapes owing to Doppler broadening and pressure broadening, respectively. The Doppler width can be readily calculated for a given temperature [33]. The line-integral of the absorption cross-section can be calculated from the transition probability, A_i , and the degeneracies of the upper, g'_i , and lower, g''_i , states:

$$\int_0^\infty \sigma_i(\nu) d\nu = \frac{g'_i}{g''_i} \frac{A_i}{8\pi c \nu_i^2} \left(1 - \exp\left(\frac{-hc\nu_i}{kT}\right) \right) \tag{4}$$

where T is the temperature, k is the Boltzmann constant, h is Planck's constant and c is the speed of light in a vacuum. Note that the exponential term in Eq. 4, which accounts for stimulated emission, is essentially negligible for the probed transition at the prevailing temperature. The number density in the ground state of each transition is related to the mole fraction of acetylene, $x_{C_2H_2}$, via

$$N_i = \frac{g''_i \exp\left(\frac{-hcE''_i}{kT}\right)}{Q(T)} x_{C_2H_2} N \tag{5}$$

where $Q(T)$ is the partition function of acetylene, E''_i is the transition ground state energy and N is the overall number density determined from the ideal gas law. The partition function for acetylene is tabulated in the HITRAN database for a broad temperature range [34]. A polynomial was fitted to this data for the purpose of evaluating $Q(T)$ during spectral fitting. Relevant data for the P17e and P7e acetylene lines are shown in Table 1.

The linewidth of the Lorentzian component of the line shape mentioned above cannot be accurately determined from theory. The HITRAN database tabulates measured collisional broadening parameters for various gases, including acetylene, at ambient temperature. It also lists power-law exponents characterising the temperature-dependence of these collisional broadening parameters, but these are not intended for extrapolation to very high

Table 1 Spectroscopic parameters for the P7e and P17e lines used in fitting model spectra to experimental data (variables are defined in the text) [34]

	ν_i/cm^{-1}	A_i/s^{-1}	E''_i/cm^{-1}	g'_i	g''_i
P7e	6512.825	4.76	677.5067	39	45
P17e	6512.992	5.22	359.9015	99	105

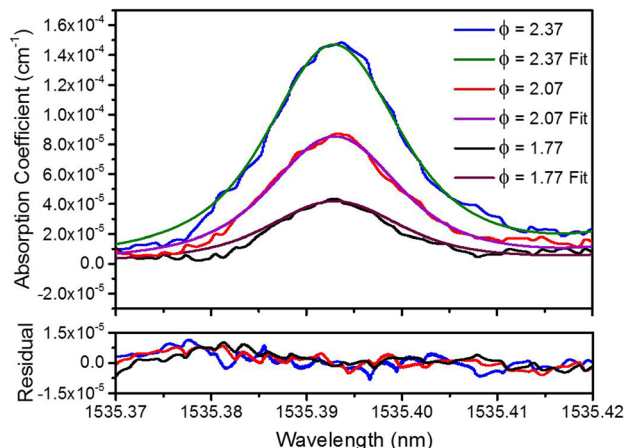


Fig. 4 Subtracted spectra of P17e line of acetylene, recorded 2 mm above the burner surface, for a range of different flames, shown with a fit to model spectra calculated from HITRAN 2016

temperature and thus are not expected to accurately represent line broadening in flames. For this reason, the following approach was followed. Initially, the fitting algorithm was used for spectra measured in the $\phi = 2.37$ flame and at 2 mm above the burner, where the acetylene concentration is highest. In this initial step, there were three floating parameters: (1) concentration of acetylene; (2) location of the peak of the P17e line (to establish the absolute wavelength scale as described above); (3) the full-width at half-maximum (FWHM) of the Lorentzian contribution to the Voigt profiles. The average total collisional broadening parameter for three repetitions of the $\phi = 2.37$ spectrum at 2 mm above the burner was thus estimated as, $\Delta\nu_L = 0.0551 \text{ cm}^{-1}$. For data obtained at all other positions and equivalence ratios, this value for the collisional broadening parameter was used as a fixed parameter in the model. This is considered to be justified since the composition and temperature downstream of the reaction zone in the rich set of flames studied will be subject to only minor variation, with nitrogen as the dominant collision partner throughout. Accordingly, the spectra fitted to all the other experimental spectra included just one floating parameter, which was the acetylene concentration. Example fits of the model to experimental spectra recorded at 2 mm above the burner surface are shown in Fig. 4.

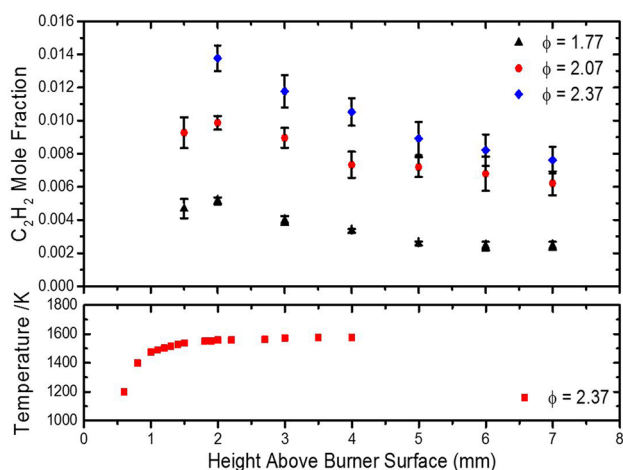


Fig. 5 (Upper plot) Measured concentrations of acetylene as a function of height above the burner surface. Error bars represent the standard error of the mean based on three repetitions of the measurements. (Lower plot) Temperature measurements by OH excitation thermometry in a $\phi = 2.37$ flame

4 Results

Figure 5 shows the recovered acetylene mole fractions at 1 mm increments of height above burner for a range of flames with different equivalence ratios. The error bars represent the standard error of the mean, calculated based on three repetitions for each data-point, to indicate the precision of the measurements. Higher equivalence ratio flames exhibit a greater peak concentration of acetylene. The measured acetylene concentration decays with increasing height above burner, which could be commensurate with the role of acetylene in reactions ultimately leading to the formation of PAH and soot. Previous experimental evidence, largely obtained by extractive sampling [17, 19, 35, 36], albeit in premixed flames of somewhat different composition, also corroborates the decaying trend of acetylene with increasing HAB. The technique presented here provides a methodology for non-intrusive, in situ measurements to better understand the role of acetylene in soot formation.

Shown in Fig. 5 (lower plot) are measurements of the temperature profile of the $\phi = 2.37$ flame undertaken using laser-induced fluorescence thermometry of OH, performed previously by scanning over a sequence of lines in the S_{12} band and constructing a Boltzmann plot [37]. The temperature of the $\phi = 2.37$ flame had been measured through a range of positions from 0.6 to 4 mm above the surface of the burner. These measurements were then extrapolated to higher positions by assuming a uniform temperature in the plateau region above 4 mm, where the OH LIF signal level was not sufficient for thermometry. Temperature measurements were not available for the other two flame conditions studied ($\phi = 1.77$ and $\phi = 2.07$), however, simulations

performed using Cantera lead us to expect only minor differences in temperature profile between the flames studied. Therefore, for the purpose of evaluating concentrations, the temperature profile for the $\phi = 2.37$ flame was scaled based on the difference between the simulated peak flame temperatures.

These measurements of absolute acetylene concentration are subject to a few sources of uncertainty. Due to the significant temperature-dependence of the line strength of the P17e transition, particularly at flame conditions, a calculation of the error in concentration measurements has been performed for temperature variations of ± 80 K which is estimated as the uncertainty in the temperature data. The result of this analysis shows that there is a relative uncertainty in the recovered acetylene concentration of about $\pm 27\%$. A further uncertainty in the concentration measurement arises from the confidence limits for the line strength of the P17e feature taken from the HITRAN database, which is given as $\pm 2\%$ [32, 38]. The standard error for the measurements (shown as error bars in Fig. 5) was typically around $\pm 10\%$. Although there are other potential sources of error, these are likely to be insignificant in comparison to the error arising from the temperature uncertainty. The overall measurement uncertainty is obtained as the square root of the sum of the squares of the individual uncertainties leading to an overall measurement uncertainty of $\pm 29\%$.

Measurements of the ring-down time at the off-resonance, reference wavelength (1535.34 nm) were also taken at 1 mm increments in a variety of flames. Figure 6 shows the extinction coefficient at each position. In this case, the ring-down time of the cavity in the absence of the flame was used as the basis for τ_0 . The average ring-down time for the empty cavity was 37.5 μ s and the longest ring-down time recorded with the flame intra-cavity was 12.7 μ s. It is clearly observed that the higher equivalence ratio flames have a higher level of broadband optical loss. There are additional losses at

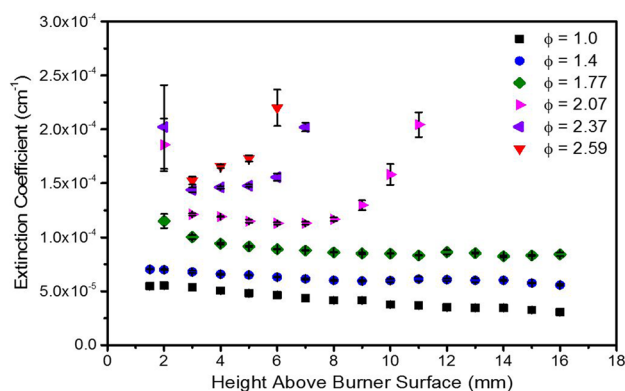


Fig. 6 Extinction coefficient as a function of height above the burner surface. Error bars represent the standard error of the mean based on three repetitions of the measurements

higher positions in the flames which produce soot ($\phi = 2.07$, $\phi = 2.37$ and $\phi = 2.59$). Interestingly, for the $\phi = 2.37$ and $\phi = 2.59$ flames, these losses are present at lower positions than soot has been measured previously using laser-induced incandescence (LII) or photoacoustic methods [39].

5 Discussion

The measurements of extinction coefficient at the reference wavelength show increased broadband extinction with increasing equivalence ratio. This is thought to be primarily due to the increasing concentration of polycyclic aromatic hydrocarbons (PAHs) in the richer flames. These species have a large number of ro-vibrational transitions due to their complexity, leading at flame temperature to near-continuum broadband absorption in the NIR region. In flames with a low soot volume fraction, there is no significant change in the extinction coefficient with height above the burner surface. However, for higher equivalence ratio flames (those with $\phi = 2.07$ or greater), there is a significant upturn in the extinction coefficient above a certain point in the flame. For the two richest flame conditions ($\phi = 2.37$ and $\phi = 2.59$), this occurs far upstream of the onset of soot formation, which is known from previous research to occur at around 8 mm [39]. This seems to indicate the presence of a large reservoir of PAHs at these upstream locations. By contrast, for the $\phi = 2.07$ flame, the apparent rise in extinction corresponds with the onset of soot formation at 8 mm.

Interestingly, for the $\phi = 1.77$ case, which is close to the ‘nucleation flame’ conditions investigated by others [6, 40–42], and therefore, just above the threshold for soot formation, no increase in extinction with increasing HAB is observed, despite the sensitivity of the technique. The apparent increase in extinction for the richer flames, at the lowest vertical positions, can be attributed to the reaction zone being located slightly further above the burner (due to the lower adiabatic flame speed), causing the edge of the steep vertical temperature gradient to perturb the beam in the cavity. Indeed, due to these thermal effects low down in the flame, it was not possible to obtain satisfactory concentration measurements of acetylene at 1.5 mm HAB for the richest flame as seen in Fig. 5. The measurements at this location for the other flames show larger error bars than elsewhere for the same reason and it was not possible to obtain measurements below 1.5 mm HAB.

Turning to the practicalities of implementing the technique reported here, it should be noted that the presence of the flame in the cavity has some implications for the data acquisition rate, when compared with cw-CRDS performed at ambient conditions. The typical measurement repetition rate for the flame measurements reported above was 4 Hz, which is a significant reduction compared to the 100 Hz

which could ideally be achieved using the 50 Hz cavity length modulation frequency. This is due to the broadband losses limiting the on-resonance cavity transmission, with the majority of the resonances failing to achieve the threshold to trigger a ring-down measurement. Despite the reduction in the mode-matching efficiency to the TEM_{00} mode due to thermo-optical effects of the flame, which causes an increase in the coupling efficiency of the input light into higher-order transverse modes, the TEM_{00} is still preferentially excited. Maintaining the trigger level at a suitably high level ensures that ring-down measurements are only made using the TEM_{00} mode, although at the expense of increased acquisition time. As such, the actual time taken to acquire a ring-down time spectrum of acetylene over the measurement wavelength range (1535.30–1535.55 nm) was relatively slow, especially for richer flames at higher measurement positions above the burner surface due to the strong broadband losses. For instance, it took 20 min and 80 min, respectively, to acquire ring-down time spectra in a $\phi = 2.37$ flame at measurement positions of 2 mm and 7 mm. As noted above, the acquisition time for concentration measurements could be reduced significantly by scanning only over the narrower wavelength region used for spectral fitting. Overall, the measurements achieved good signal-to-noise ratio (SNR). The SNR for the P17e absorption peak was calculated by comparing the standard deviation of the ring-down time at the reference wavelength with the ring-down time at the wavelength of the peak absorption feature. This resulted in an SNR of 43 for the spectrum recorded in the $\phi = 2.37$ flame at 2 mm above the burner surface and a detection limit of $9.4 \times 10^{-6} \text{ cm}^{-1}$ (3σ).

6 Conclusion

Continuous-wave cavity ring-down spectroscopy has been applied to in situ measurements of acetylene in a range of flat flames. Our previously reported experimental methodology has been modified in this work to exclude the use of a second DFB laser and an optical switching system. A reference region of negligible narrow-band absorption has been identified to obtain the off-resonance measurements used for normalising the measured spectra. We show a methodology for recovering acetylene concentration from the measured spectra, and the recovered profiles show a decaying trend of acetylene concentration with HAB, which is consistent with the consumption of acetylene in reactions forming PAHs and ultimately soot. Extinction results reveal significant broadband optical losses in the richer flames, including prior to the onset of soot formation, which may be partly attributable to near-infrared absorption by aromatic species.

Acknowledgements The authors gratefully acknowledge funding from the UK Engineering and Physical Sciences Research Council (EPSRC), Platform Grant EP/P001661/1. P.O. was in receipt of a PhD studentship from the University of Strathclyde. G.H. was supported by an EPSRC Doctoral Prize.

Author contributions P.O. performed the cw-CRDS experiments, analysed the data and prepared the figures, with support from G.H.; Y.H. performed the flame temperature measurements; I.B. and M.L. supervised the research; P.O. and G.H. drafted the manuscript; I.B. edited the manuscript with additional contributions from M.L.

Declarations

Conflict of interest The authors have no competing interests to declare that are relevant to the content of this article.

References

1. E. Samoli et al., Associations of short-term exposure to traffic-related air pollution with cardiovascular and respiratory hospital admissions in London, UK. *Occup. Environ. Med.* **73**(5), 300–307 (2016)
2. W.-J. Guan et al., Impact of air pollution on the burden of chronic respiratory diseases in China: time for urgent action. *Lancet* **388**(10054), 1939–1951 (2016)
3. L. Drinovec et al., The “dual-spot” Aethalometer: an improved measurement of aerosol black carbon with real-time loading compensation. *Atmos. Meas. Tech.* **8**(5), 1965–1979 (2015)
4. H. Wang, Formation of nascent soot and other condensed-phase materials in flames. *Proc. Combust. Inst.* **33**(1), 41–67 (2011)
5. H.A. Michelsen, Probing soot formation, chemical and physical evolution, and oxidation: a review of in situ diagnostic techniques and needs. *Proc. Combust. Inst.* **36**(1), 717–735 (2017)
6. P. Desgroux et al., Comparative study of the soot formation process in a “nucleation” and a “sooting” low pressure premixed methane flame. *Combust. Flame* **184**, 153–166 (2017)
7. E.K. Yapp et al., Numerical simulation and parametric sensitivity study of optical band gap in a laminar co-flow ethylene diffusion flame. *Combust. Flame* **167**, 320–334 (2016)
8. H. Richter, J.B. Howard, Formation of polycyclic aromatic hydrocarbons and their growth to soot—a review of chemical reaction pathways. *Prog. Energy Combust. Sci.* **26**(4), 565–608 (2000)
9. J.A. Miller, C.F. Melius, Kinetic and thermodynamic issues in the formation of aromatic compounds in flames of aliphatic fuels. *Combust. Flame* **91**(1), 21–39 (1992)
10. S. Wagner et al., TDLAS-based in situ measurement of absolute acetylene concentrations in laminar 2D diffusion flames. *Proc. Combust. Inst.* **32**(1), 839–846 (2009)
11. F. Fuest et al., Quantitative acetylene measurements in laminar and turbulent flames using 1D Raman/Rayleigh scattering. *Combust. Flame* **162**(5), 2248–2255 (2015)
12. B.A. Williams, J.W. Fleming, Laser-induced fluorescence detection of acetylene in low-pressure propane and methane flames. *Appl. Phys. B* **75**(8), 883–890 (2002)
13. R.P. Lucht, R.L. Farrow, R.E. Palmer, Acetylene measurements in flames by coherent anti-stokes Raman scattering. *Combust. Sci. Technol.* **45**(5–6), 261–274 (1986)
14. Z.S. Li et al., Mid-infrared polarization spectroscopy of C₂H₂: non-intrusive spatial-resolved measurements of polyatomic hydrocarbon molecules for combustion diagnostics. *Proc. Combust. Inst.* **31**(1), 817–824 (2007)
15. Z.W. Sun et al., Quantitative C₂H₂ measurements in sooty flames using mid-infrared polarization spectroscopy. *Appl. Phys. B* **101**(1), 423–432 (2010)
16. J.J. Scherer et al., Determination of methyl radical concentrations in a methane/air flame by infrared cavity ringdown laser absorption spectroscopy. *J. Chem. Phys.* **107**(16), 6196–6203 (1997)
17. S. Gersen, A.V. Mokhov, H.B. Levinsky, Extractive probe/TDLAS measurements of acetylene in atmospheric-pressure fuel-rich premixed methane/air flames. *Combust. Flame* **143**(3), 333–336 (2005)
18. J.H. Miller et al., Measurements of hydrogen cyanide and its chemical production rate in a laminar methane/air, non-premixed flame using cw cavity ringdown spectroscopy. *Proc. Combust. Inst.* **29**, 2203–2209 (2002)
19. B. Apicella et al., The effect of temperature on soot properties in premixed ethylene flames. *Combust. Sci. Technol.* **191**(9), 1558–1570 (2019)
20. A.M. Bennett et al., Soot formation in laminar flames of ethylene/ammonia. *Combust. Flame* **220**, 210–218 (2020)
21. C. Saggese et al., Probe effects in soot sampling from a burner-stabilized stagnation flame. *Combust. Flame* **167**, 184–197 (2016)
22. N. Hansen et al., Investigation of sampling-probe distorted temperature fields with X-ray fluorescence spectroscopy. *Proc. Combust. Inst.* **37**(2), 1401–1408 (2019)
23. N. Hansen et al., 2D-imaging of sampling-probe perturbations in laminar premixed flames using Kr X-ray fluorescence. *Combust. Flame* **181**, 214–224 (2017)
24. N. Lamoureux, P. Desgroux, In situ laser-induced fluorescence and ex situ cavity ring-down spectroscopy applied to NO measurement in flames: microprobe perturbation and absolute quantification. *Energy Fuels* **35**(9), 7107–7120 (2021)
25. G.S. Humphries, I.S. Burns, M. Lengden, Application of continuous-wave cavity ring-down spectroscopy to laminar flames. *IEEE Photonics J.* **8**(1), 3900110 (2016)
26. H. Huang, K.K. Lehmann, CW cavity ring-down spectroscopy (CRDS) with a semiconductor optical amplifier as intensity modulator. *Chem. Phys. Lett.* **463**(1–3), 246–250 (2008)
27. W. Johnstone et al., Tunable diode laser spectroscopy for industrial process applications: system characterization in conventional and new approaches. *IEEE Sens. J.* **8**(7), 1079–1088 (2008)
28. B. Axelsson, R. Collin, P.-E. Bengtsson, Laser-induced incandescence for soot particle size measurements in premixed flat flames. *Appl. Opt.* **39**(21), 3683–3690 (2000)
29. C. Schulz et al., Laser-induced incandescence: recent trends and current questions. *Appl. Phys. B* **83**(3), 333–354 (2006)
30. K.K. Lehmann, G. Berden, R. Engeln, An introduction to cavity ringdown spectroscopy, in *Cavity Ringdown Spectroscopy: Techniques and Applications*, G. Berden and R. Engeln (eds.), pp. 1–26 (Blackwell, Chichester, 2009)
31. L.S. Rothman et al., HITEMP, the high-temperature molecular spectroscopic database. *J. Quant. Spectrosc. Radiat. Transf.* **111**(15), 2139–2150 (2010)
32. I.E. Gordon et al., The HITRAN2016 molecular spectroscopic database. *J. Quant. Spectrosc. Radiat. Transf.* **203**, 3–69 (2017)
33. A.C. Eckbreth, *Laser Diagnostics for Combustion Temperature and Species*, 2nd edn. Combustion Science and Technology. (Gordon and Breach Publishers, Amsterdam, 1996)
34. L.S. Rothman et al., The HITRAN2012 molecular spectroscopic database. *J. Quant. Spectrosc. Radiat. Transf.* **130**, 4–50 (2013)
35. E. Kaiser et al., Experimental and modeling study of premixed atmospheric-pressure dimethyl ether—air flames. *J. Phys. Chem. A* **104**(35), 8194–8206 (2000)
36. S.P. Roy, D.C. Haworth, A systematic comparison of detailed soot models and gas-phase chemical mechanisms in laminar premixed flames. *Combust. Sci. Technol.* **188**(7), 1021–1053 (2016)

37. Y. Hu, Radical concentration and temperature measurements in sooting flames by cavity ringdown spectroscopy and laser-induced fluorescence, PhD thesis (University of Strathclyde, Glasgow, 2015)
38. R. El Hachtouki, J. Vander Auwera, Absolute line intensities in acetylene: the 1.5- μm region. *J. Mol. Spectrosc.* **216**(2), 355–362 (2002)
39. G.S. Humphries et al., In situ photoacoustic measurement of soot profiles in laminar flames using a high-repetition-rate pulsed fibre laser. *Appl. Phys. B* **125**(4), 60 (2019)
40. C. Betrancourt et al., Investigation of the size of the incandescent incipient soot particles in premixed sooting and nucleation flames of n-butane using LII, HIM, and 1 nm-SMPS. *Aerosol. Sci. Technol.* **51**(8), 916–935 (2017)
41. H. Bladh et al., Probing the smallest soot particles in low-sooting premixed flames using laser-induced incandescence. *Proc. Combust. Inst.* **35**(2), 1843–1850 (2015)
42. A. Ergut et al., The effect of equivalence ratio on the soot onset chemistry in one-dimensional, atmospheric-pressure, premixed ethylbenzene flames. *Combust. Flame* **151**(1), 173–195 (2007)

Publisher's Note Springer Nature remains neutral with regard to jurisdictional claims in published maps and institutional affiliations.

Springer Nature or its licensor holds exclusive rights to this article under a publishing agreement with the author(s) or other rightsholder(s); author self-archiving of the accepted manuscript version of this article is solely governed by the terms of such publishing agreement and applicable law.